# Symmetry-enhanced discontinuous phase transition in a two-dimensional quantum magnet

Bowen Zhao<sup>1</sup>, Phillip Weinberg<sup>1</sup> and Anders W. Sandvik 12.2\*

In a quantum phase transition, the ground state and low-temperature properties of a system change drastically as some parameter controlling zero-point quantum fluctuations is tuned to a critical value. Like classical phase transitions driven by thermal fluctuations, a ground-state transition can be discontinuous (first order) or continuous. Theoretical studies have suggested exotic continuous transitions where a system develops higher symmetries than those of the underlying Hamiltonian. Here, we demonstrate an unconventional discontinuous transition between two ordered ground states of a quantum magnet, with an emergent symmetry of its coexistence state. We present a Monte Carlo study of a two-dimensional S = 1/2 spin system hosting an antiferromagnetic state and a plaquette-singlet solid state of the kind recently detected in  $SrCu_2(BO_3)_2$ . We show that the O(3) symmetric antiferromagnetic order and the scalar plaquette-singlet solid order form an O(4) vector at the transition. Unlike conventional first-order transitions, there are no energy barriers between the two coexisting phases, as the O(4) order parameter can be rotated at constant energy. Away from the transition, the O(4) surface is uniaxially deformed by the control parameter (a coupling ratio). This phenomenon may be observable in  $SrCu_2(BO_3)_2$ .

heoretical studies of exotic quantum states of matter and the phase transitions between them can provide new perspectives on many-body physics and stimulate experimental investigations. A prominent example is the quantum phase transition between antiferromagnetic (AFM) and spontaneously dimerized valence-bond solid (VBS) ground states in two-dimensional (2D) spin S=1/2 magnets<sup>1,2</sup>. Here the theory of deconfined quantum critical points (DQCPs) suggests that the Landau-Ginzburg-Wilson (LGW) paradigm for phase transitions is inapplicable, as a consequence of quasiparticle fractionalization<sup>3,4</sup>. Over the past decade, likely DQCPs have been identified in lattice models, using 'designer Hamiltonians' constructed for their amenability to largescale quantum Monte Carlo (QMC) simulations of the AFM-VBS transition<sup>5-16</sup>. Recently, a potential experimental realization of this type of DQCP was reported in the quasi-2D Shastry-Sutherland (SS) compound SrCu<sub>2</sub>(BO<sub>3</sub>)<sub>2</sub> under pressure<sup>17</sup>. Although the SS model<sup>18</sup> (Fig. 1a) is difficult to study numerically due to its geometrical frustration (which causes sign problems in QMC simulations), a specific type of VBS—a two-fold degenerate plaquette-singlet solid (PSS) located between AFM and bond-singlet phases—was demonstrated convincingly by tensor-network calculations<sup>19</sup>. It has been suggested<sup>17</sup> that the AFM-PSS transition in SrCu<sub>2</sub>(BO<sub>3</sub>)<sub>2</sub> may be a DQCP. It is not immediately clear, however, if the two-fold degenerate PSS can support spinon deconfinement in the same way as a four-fold degenerate VBS. QMC studies of rectangular lattices with two-fold degenerate VBS states point to a first-order transition<sup>13</sup>, as was also found in the SS model<sup>19</sup>.

Here we study a QMC sign-free model that mimics the SS compound, sharing the same kinds of AFM and PSS ground states. The model [Fig. 1b], is a new member in the '*J-Q*' family<sup>5</sup>, with Heisenberg exchange *J* supplemented by four-spin interactions *Q* that weaken and eventually destroy the AFM order. Our QMC simulations demonstrate an unconventional discontinuous AFM–PSS transition with emergent O(4) symmetry of the coexistence state.

Non-LGW critical points with emergent symmetries have been extensively investigated recently<sup>20–30</sup>. In the case discussed here, the transition is first-order, in the sense that the order parameters exhibit clear discontinuities. However, conventional coexistence of phases separated by an energy barrier is not observed. Using order-parameter distributions, we show that the phase coexistence at the transition takes the form of an O(4) symmetric vector arising out of the O(3) AFM and scalar ( $Z_2$ ) PSS order parameters, even though there is no microscopic symmetry relating the two different order parameters in this way. The emergent order parameter can be arbitrarily O(4) rotated at constant energy. In further support of this striking scenario, we demonstrate a characteristic logarithmic form of the PSS ordering temperature versus the tuning parameter, as expected for a 2D uniaxially deformed O( $N \ge 3$ ) quantum system<sup>31,32</sup>.

### **Ground states**

Our Hamiltonian can be defined using singlet projection operators  $P_{ii} = (1/4 - \mathbf{S}_i \cdot \mathbf{S}_i)$ :

$$H = -J \sum_{\langle ij \rangle} P_{ij} - Q \sum_{ijkl \in \square'} (P_{ij} P_{kl} + P_{ik} P_{jl})$$

$$\tag{1}$$

where all indicated site pairs comprise nearest neighbours on a periodic square lattice with  $L^2$  sites and  $\Box'$  denotes the  $2 \times 2$  Q-plaquettes in Fig. 1b. For  $g = J/Q \rightarrow \infty$ , this chequerboard J - Q (CBJQ) model reduces to the usual AFM Heisenberg model, and for  $g \rightarrow 0$  we will demonstrate a two-fold degenerate PSS. The model does not have any phase corresponding to the large-J'/J bond-singlet state of the SS model. However, for the AFM-PSS transition we can invoke symmetries and universality to propose that the two models, as well as  $SrCu_2(BO_3)_2$ , contain the same physics.

We use two different QMC methods to study the CBJQ model: ground-state projection in the basis of valence bonds<sup>33</sup> and the stochastic series expansion (SSE) method<sup>34</sup>. Both techniques

NATURE PHYSICS ARTICLES

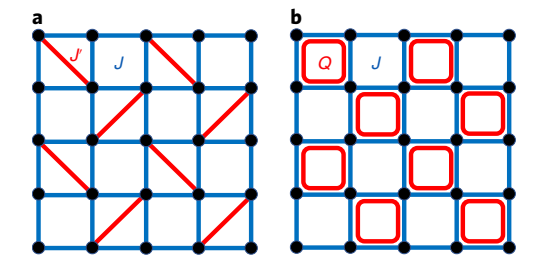


**Fig. 1 | Quantum spin models discussed in this work. a,** In the SS model, nearest-neighbour Heisenberg interactions *J* compete with next-nearest-neighbour couplings (diagonal lines). **b,** In the CBJQ model, the *J'* terms are replaced by the four-spin *O* terms in equation (1).

deliver results without any approximations other than statistical errors. The projector method is used for T=0 spin-rotationally averaged quantities, while the SSE method is more efficient for  $S^z$ -basis observables when the temperature is scaled as  $T \propto 1/L$ , as appropriate for finite-size scaling at a quantum phase transition with dynamic exponent z=1 and also for a first-order transition. Both QMC techniques are further described in the Methods.

To demonstrate a PSS ground state we first study a conventional dimer order parameter

$$D_{\mu} = \frac{1}{L^2} \sum_{\mathbf{r}} (-1)^{r_{\mu}} \mathbf{S}(\mathbf{r}) \cdot \mathbf{S}(\mathbf{r} + \hat{\mu}), \quad \hat{\mu} = \hat{x}, \hat{y}$$
 (2)

where  $\mathbf{r} = (r_x, r_y)$ . In a VBS,  $\langle D_x \rangle \neq 0$ ,  $\langle D_y \rangle = 0$  for x-oriented bond order and  $x \leftrightarrow y$  for the y orientation. Because a singlet plaquette can be regarded as a resonance between horizontal and vertical bond pairs, a two-fold degenerate PSS (with higher singlet density on even or odd rows in in Fig. 1) should have  $|\langle D_x \rangle| = |\langle D_y \rangle| \neq 0$ . On a finite lattice the symmetry is not broken, and the system fluctuates between the two states. We use the projector method to generate the probability distribution  $P(D_x, D_y)$ . While strictly not a quantum mechanical observable, this distribution nevertheless properly reflects the fluctuations and symmetries of the system. Results on either side of the AFM–PSS transition (the location of which will be determined below) are shown in Fig. 2. We see the two-fold symmetry of a PSS, instead of the four-fold symmetry of the columnar VBS<sup>9,35</sup>.

In the original J-Q model with Q terms on all plaquettes, the AFM-VBS transition appears to be continuous<sup>16</sup> and, in accord with the DQCP theory, an emergent U(1) symmetry of its microscopically  $Z_4$  invariant VBS order parameter has been confirmed<sup>5,7,35</sup>. The proposed field theory description with spinons coupled to an U(1) gauge field<sup>3,4</sup> therefore seems viable. Unusual finite-size scaling behaviours not contained within the theory (but not contradicted by it) have also been observed 10,15,16 (and interpreted by some as a weak first-order transition<sup>7,8,11</sup>). An interesting proposal is that the O(3) symmetry of the AFM and the emergent U(1) symmetry of the VBS may combine into an SO(5) symmetry exactly at the critical point<sup>20,36</sup>. In a spin-planar J-Q model, it has instead been demonstrated that the U(1) AFM order parameter and the emergent U(1) VBS symmetry combine into a emergent O(4) symmetry<sup>26</sup>. In yet another example, it was proposed that a system with O(3) AFM order and Z<sub>2</sub> Kekule VBS state exhibits a DQCP with emergent SO(4) symmetry<sup>27</sup>. The O(3) and  $Z_2$  symmetries apply also to the CBJQ model, and we therefore pay attention to a potential O(4) or SO(4) symmetry (and we cannot distinguish between these, as we only test for the rotational symmetry).

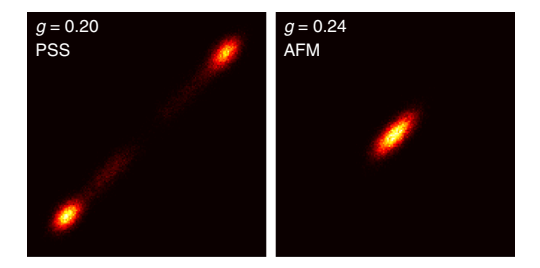


**Fig. 2** | **Demonstration of a two-fold degenerate PSS state.** The distribution  $P(D_x, D_y)$  in the ground state of the CBJQ model is shown at g = 0.20 (PSS phase) and g = 0.24 (AFM phase). The results were obtained in projector QMC simulations on L = 96 lattices.

#### Finite-size scaling

To analyse the AFM–PSS transition we perform SSE calculations at T = 1/L and use order parameters defined solely with the  $S^z$  spin components:

$$m_z = \frac{1}{L^2} \sum_{\mathbf{r}} \phi(\mathbf{r}) S^z(\mathbf{r}), \quad m_p = \frac{2}{L^2} \sum_{\mathbf{q}} \theta(\mathbf{q}) \Pi^z(\mathbf{q})$$
 (3)

where z and p mark the AFM and PSS order parameters, respectively. In  $m_z$ ,  $\mathbf{r}$  runs over all  $L^2$  lattice sites and  $\phi(\mathbf{r}) = \pm 1$  is the staggered AFM sign. In  $m_v$ , we have defined an operator

$$\Pi^{z}(\mathbf{q}) = S^{z}(\mathbf{q})S^{z}(\mathbf{q} + \hat{x})S^{z}(\mathbf{q} + \hat{y})S^{z}(\mathbf{q} + \hat{x} + \hat{y})$$
(4)

for detecting plaquette modulation, and the index  $\mathbf{q}$  runs over the lower-left corners of the Q plaquettes in Fig. 1. The signs  $\theta(\mathbf{q}) = \pm 1$  correspond to even or odd plaquette rows.

We will primarily analyse the Binder cumulants

$$U_p = \frac{3}{2} \left[ 1 - \frac{\langle m_p^4 \rangle}{3 \langle m_p^2 \rangle^2} \right], \quad U_z = \frac{5}{2} \left[ 1 - \frac{\langle m_z^4 \rangle}{3 \langle m_z^2 \rangle^2} \right]$$
 (5)

shown in Fig. 3a, where the coefficients are chosen such that, for  $L \to \infty$ ,  $U_z \to 1$ ,  $U_p \to 0$  in the AFM phase while  $U_z \to 0$ ,  $U_p \to 1$  in the PSS. If there is a single transition, we can use the crossing point at which  $U_z(g, L) = U_p(g, L)$  to define a finite-size transition point. We also study the more commonly used crossing points of curves for two different system sizes, L/2 and L, locating the g value where  $U_z(g, L/2) = U_z(g, L)$  or  $U_p(g, L/2) = U_p(g, L)$ . The three definitions should flow to the same  $g_c$  when  $L \to \infty$ .

From the slopes of the cumulants we can extract the correlationlength exponents  $\nu_z$  and  $\nu_p$  (refs.  $^{16,37}$ ):

$$\frac{1}{\nu_{zp}} = \frac{1}{\ln(2)} \ln \left( \frac{dU_{zp}(g, L) / dg}{dU_{zp}(g, L/2) / dg} \right)_{g = g_c(L)}$$
(6)

where  $g_c(L)$  is the relevant (L/2, L) cross point. The derivatives can be evaluated directly in the QMC simulations.

The analysis is presented and explained in Fig. 3. We find  $g_c = 0.2175 \pm 0.0001$  from the cross point estimators in Fig. 3b. Most notably, in Fig. 3c the order parameters at their respective Binder crossing points do not vanish as  $L \to \infty$ . This coexistence of AFM and PSS order is a conventional indicator of a first-order transition. The exponents  $1/\nu_z$  and  $1/\nu_p$  provide further useful information: at a classical first-order transition,  $1/\nu \to d$  in d dimensions, and in a 2+1-dimensional quantum system we might expect  $1/\nu_{zp} \to 3$ .

ARTICLES NATURE PHYSICS

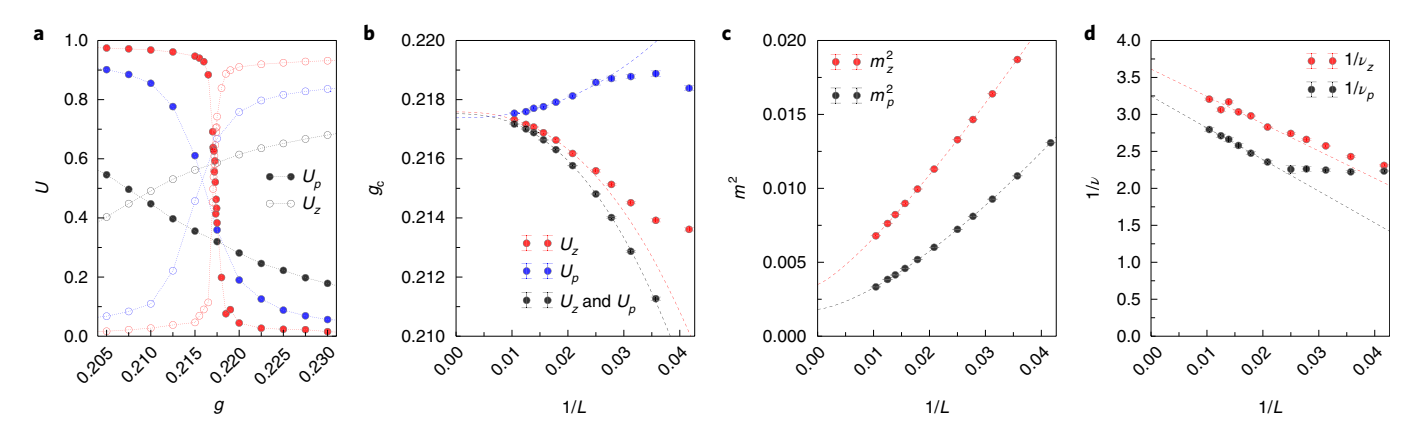


**Fig. 3 | CBJQ** results from SSE simulations. **a**, Spin (open symbols) and plaquette (filled symbols) cumulants versus g for L = 24 (black), 48 (blue) and 96 (red). Interpolations within these and additional data sets underlie the analysis presented in the other panels. **b**, Crossing g values of  $U_z$  and  $U_p$ , shown versus 1/L along with the (L/2, L) same-quantity crossing points from  $U_z$  and  $U_p$ . The fitted curves include a single power-law correction  $\alpha L^{-\omega}$  and give  $g_c = 0.2175 \pm 0.0001$  for  $L \to \infty$ . **c**, The squared order parameters at the (L/2, L) cumulant cross-points plotted versus 1/L together with polynomial fits. **d**, Correlation-length exponents (equation (6)) and line fits. Small system sizes were excluded from all fits until acceptable agreement with the functional forms were obtained. Error bars represent one standard deviation of the OMC-computed mean values.

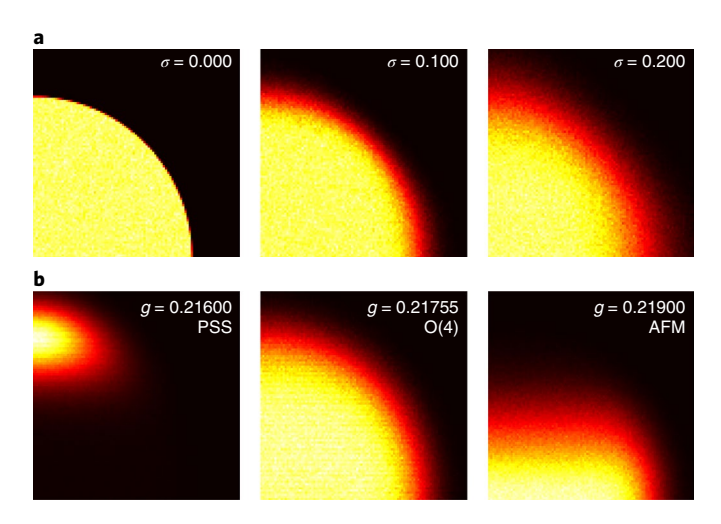


**Fig. 4 | Direct evidence for emergent O(4) symmetry. a**, One quadrant of the sampled<sup>49</sup> distribution of two components of an R = 1 O(4) vector with Gaussian length fluctuations of standard deviation  $\sigma = 0$ , 0.1, 0.2. **b**, Distribution  $P(m_z, m_p)$  for the L = 96 CBJQ model at three g values. The x and y axes represent the AFM  $m_z$  order parameter and the PSS order parameter  $m_{pr}$  respectively.

The even larger values seen in Fig. 3d indicate a particular type of discontinuous transition, as we explain in the following.

# **Emergent O(4) symmetry**

Due to the energy barrier separating coexisting phases at a conventional first-order transition, the squared order parameter follows a bimodal distribution, causing a divergent negative peak in the Binder cumulant<sup>38,39</sup>. Such peaks are present at the first-order transition in a J-Q model with a staggered  $Z_4$  VBS<sup>40</sup>, but are absent in Fig. 3a. This lack of negative cumulant peaks leads us to consider a scenario for coexisting order parameters without energy barriers in the CBJQ model.

A well-known case illustrating our proposal is the 3D XXZ-deformed Heisenberg O(3) model, with bond energies  $H_{ij} = -(\sigma_i^x \sigma_j^x + \sigma_i^y \sigma_j^y) - \Delta \sigma_i^z \sigma_j^z$  between classical spins  $\sigma_i$ ,  $\sigma_j$ . As shown in the Supplementary Information, in its ordered phase the

XXZ model behaves very similarly to the CBJQ model if we make an analogy between the planar (x-y) magnetization and the AFM order parameter on the one hand and the Ising (z) magnetization and the PSS order parameter on the other hand. Going from  $\Delta < 1$  to  $\Delta > 1$  the magnetization flips from the x-y plane to the z axis. At the O(3) point ( $\Delta = 1$ ) there are clearly no free-energy barriers between the x-y and z phases; the magnetization can be continuously rotated from the x-y plane to the z axis at constant energy.

The CBJQ model does not have any explicit higher symmetry point, but our results suggest that the O(3) AFM and the  $Z_2$  PSS combine to form an emergent O(4) symmetry at  $g_c$ . In the transition region the system can then be described by an effective deformed quantum O(4) model (XXXZ model), where the control parameter g=J/Q tunes the order parameter from the O(3) phase through the O(4) point into the  $Z_2$  phase. In the thermodynamic limit, the O(4) symmetry is spontaneously broken at  $g_c$ , and the PSS and AFM orders can coexist in the same spatial region, unlike the phase separation characterizing conventional coexistence.

To test more explicitly for emergent O(4) symmetry, we use the projector QMC method and now define the PSS order parameter with the rotationally invariant operator

$$\Pi(\mathbf{q}) = [\mathbf{S}(\mathbf{q}) \cdot \mathbf{S}(\mathbf{q} + \hat{\mathbf{x}})][\mathbf{S}(\mathbf{q} + \hat{\mathbf{y}}) \cdot \mathbf{S}(\mathbf{q} + \hat{\mathbf{y}} + \hat{\mathbf{x}})] + [\mathbf{S}(\mathbf{q}) \cdot \mathbf{S}(\mathbf{q} + \hat{\mathbf{y}})][\mathbf{S}(\mathbf{q} + \hat{\mathbf{x}}) \cdot \mathbf{S}(\mathbf{q} + \hat{\mathbf{x}} + \hat{\mathbf{y}})]$$
(7)

in place of  $\Pi^z(\mathbf{q})$  in equation (3). For the AFM phase, we still use  $m_z$  in equation (3). In a state with both AFM and PSS order, the commutator  $[m_z, m_p] \propto L^{-2}$ , and we can safely use the c numbers corresponding to  $m_z$  and  $m_p$  from a given transition graph<sup>33</sup> to accumulate the distribution  $P(m_z, m_p)$ . For the putative O(4) symmetry to be manifest, we further normalize  $m_z$  and  $m_p$  by factors involving  $\langle m_z^2 \rangle$  and  $\langle m_p^2 \rangle$  (see Supplementary Information).

For points uniformly distributed on an O(4) sphere of radius R, projection onto two components results in a uniform distribution within a circle of radius R. In a finite quantum system we also expect fluctuations of R and therefore compare our CBJQ results with distributions obtained from an O(4) sphere with mean radius R=1 and different standard deviations  $\sigma$ . Examples are shown Fig. 4. At the AFM–PSS transition, the CBJQ distribution is rotation symmetric with radial profile similar to O(4) sampling with  $\sigma \approx 0.15$ . Inside the phases the distributions are shifted as expected; deep in the PSS we

NATURE PHYSICS ARTICLES

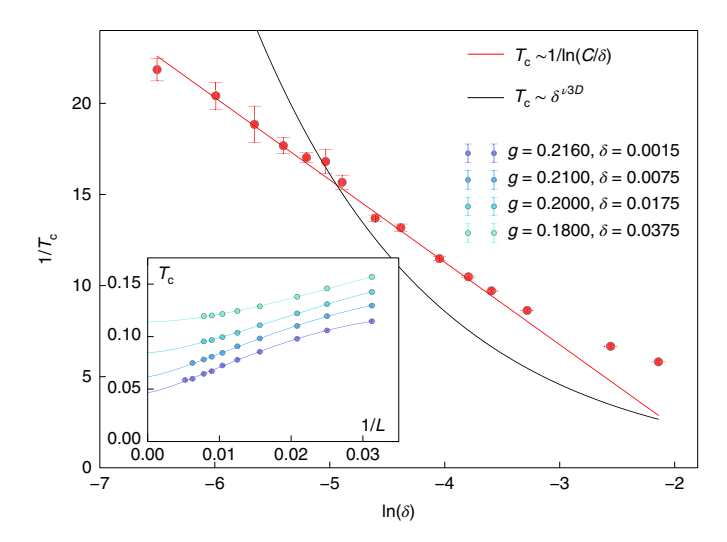


**Fig. 5 | Inverse PSS critical temperature versus the shifted coupling**  $\delta = g_c - g$ . The red line is a fit to the expected log form and the black curve shows the conventional Ising form as a contrast. Inset: examples of  $T_c$  extrapolations using the form  $T_c = aL^{-b}(1+cL^{-d})$ , with fitting parameters a, b, c and d. Error bars represent one standard deviation of the sampled mean values.

should eventually, for  $L \to \infty$ , obtain a point on the y axis, and in the AFM state a line on the x axis. Quantitative tests of the symmetry are presented in the Supplementary Information. As expected for an emergent symmetry, we find O(4) violations for small system sizes (L=8, 16), but no detectable deviations at  $g_c$  for the largest systems (up to L=96).

The O(4) symmetry explains why  $1/\nu_{z,p}>3$  in Fig. 3b. The dynamic exponent of the Anderson–Goldstone rotor states associated with the O( $N \ge 2$ ) order is z=2, and the exponents should therefore tend to d+z=4 when  $L\to\infty$  at T=0. The deviations may be due to scaling corrections and T>0 effects when  $T \propto 1/L$  (instead of  $1/L^2$ ). As we show in the Supplementary Information, quantitative measures of the emergent O(4) symmetry in our T=0 calculations exhibit  $1/L^4$  scaling of the size of the g window in which the symmetry is emergent.

An important consequence of O(4) symmetry should be a specific logarithmic (log) form of the critical PSS temperature  $T_c$  versus the distance  $\delta = g_c - g$  from the T = 0 transition point,  $T_c \propto \ln^{-1}(C/\delta)$ , as in an O( $N \ge 3$ ) model with Ising deformation 31,32. This form is very different from that expected close to an Ising quantum-critical point, where  $T_c \propto \delta^{\nu_{3D}}$ , where  $\nu_{3D}$  is the 3D Ising correlation-length exponent. Neither form should apply at a conventional first-order transition extending from ( $g_c$ , T = 0) to some T > 0. If the O(4) breaking perturbation is very weak, one should still expect the log form to hold down to some low temperature.

We computed  $T_c(g)$  for the PSS using the cumulant-crossing method with SSE data for  $L \le 160$ . We can reliably extrapolate  $T_c$  to the thermodynamic limit for  $g \le 0.216$  ( $\delta \gtrsim 0.0015$ ), as shown in Fig. 5. The behaviour for  $\delta \lesssim 0.02$  is very well described by the log form, lending strong indirect support to the emergent O(4) symmetry through an important physical observable in the thermodynamic limit.

# Discussion

To exclude the CBJQ model being fine-tuned accidentally, we also confirmed the O(4) symmetry in a model with additional interactions (see Supplementary Information). It is possible that the O(4) symmetry is present only up to some length scale above the largest system (L=96) studied here, in which case energy barriers between the AFM and PSS states would eventually form for larger systems.

Such approximate symmetries may be expected at certain weak first-order transitions, either when the system is close to a fine-tuned point with the higher symmetry (although no convincing symmetries were observed in numerical studies<sup>41</sup>) or in the proximity of a quantum-critical point where the higher symmetry is emergent<sup>20,25,28</sup>. In the latter case, perturbations break the symmetry above some length scale  $\xi'$  exceeding the correlation length  $\xi$  (ref. <sup>25</sup>).

In the CBJQ model the observed discontinuities are rather strong. In Fig. 3c the magnitude of the O(4) vector in AFM units is  $m_s = \langle 4m_z^2 \rangle^{1/2} \approx 0.12$ , almost 25% of the maximum staggered magnetization 1/2. The discontinuous nature of the transition is apparent even on small lattices, for example, the flow of  $1/\nu_z$  toward an anomalously large value in Fig. 3d. Thus, in the scenario of ref. 25 we should have  $\xi \ll L \ll \xi' \sim \xi^{1+\alpha}$ , with a large  $\alpha$  in order to have the clear separation of length scales needed to account for our observations. Such behaviour had not been anticipated previously; rather, emergent symmetry on large length scales was cited as support for continuous non-LGW transitions 20,27

In the alternative scenario of an asymptotically exact O(4) symmetry, the dominant symmetry-breaking field is tuned to zero at the AFM-PSS transition and higher-order O(4) violating perturbations would be absent or vanish upon renormalization, perhaps by an extension of the DQCP framework. Although emergent O(N) multicritical points arising from O(N-1) and  $Z_2$  order parameters have been extensively discussed within the LGW framework<sup>42-45</sup>, the influence of the higher symmetry on associated first-order lines has not been addressed until recently in the weakly first-order DQCP context<sup>25</sup>.

The T>0 Ising transition would be a good target for detecting the still incompletely characterized PSS phase in  $SrCu_2(BO_3)_2$  and its putative O(4) symmetry. In 2D we have demonstrated a log form of  $T_c$  (Fig. 5), which should hold down to some low temperature also in the presence of sufficiently weak interlayer couplings. Presumably the 3D T=0 transition is a conventional first-order one, but an approximate higher symmetry may still persist.

The O(4) AFM–PSS transition is reminicent of the SO(5) theory of high- $T_c$  superconductivity<sup>16</sup>, where O(3) AFM and O(2) superconducting order parameters form the higher symmetry—a scenario not confirmed experimentally. After completion of the present work, an SO(5) analogue of the AFM–PSS was demonstrated in a spin-1 J–Q model<sup>47</sup>, and an O(4) transition very similar to ours was discussed in the context of a classical 3D loop model<sup>48</sup>.

# Online content

Any methods, additional references, Nature Research reporting summaries, source data, statements of data availability and associated accession codes are available at https://doi.org/10.1038/s41567-019-0484-x.

Received: 1 May 2018; Accepted: 23 February 2019; Published online: 8 April 2019

#### References

- 1. Sachdev, S. Quantum magnetism and criticality. Nat. Phys. 4, 173-185 (2008).
- Kaul, R. K., Melko, R. G. & Sandvik, A. W. Bridging lattice-scale physics and continuum field theory with quantum Monte Carlo simulations. *Annu. Rev. Condens. Matter Phys.* 4, 179–215 (2013).
- Senthil, T., Vishwanath, A., Balents, L., Sachdev, S. & Fisher, M. P. A. Deconfined quantum critical points. Science 303, 1490–1494 (2004).
- Senthil, T., Balents, L., Sachdev, S., Vishwanath, A. & Fisher, M. P. A. Quantum criticality beyond the Landau–Ginzburg–Wilson paradigm. *Phys. Rev. B* 70, 144407 (2004).
- Sandvik, A. W. Evidence for deconfined quantum criticality in a two-dimensional Heisenberg model with four-spin interactions. *Phys. Rev. Lett.* 98, 227202 (2007).
- Melko, R. G. & Kaul, R. K. Scaling in the fan of an unconventional quantum critical point. *Phys. Rev. Lett.* 100, 017203 (2008).
- Jiang, F.-J., Nyfeler, M., Chandrasekharan, S. & Wiese, U.-J. From an antiferromagnet to a valence bond solid: evidence for a first-order phase transition. J. Stat. Mech. 2008, P02009 (2008).

ARTICLES NATURE PHYSICS

- Kuklov, A. B., Matsumoto, M., Prokof'ev, N. V., Svistunov, B. V. & Troyer, M. Deconfined criticality: generic first-order transition in the SU(2) symmetry case. *Phys. Rev. Lett.* 101, 050405 (2008).
- Lou, J., Sandvik, A. W. & Kawashima, N. Antiferromagnetic to valence-bondsolid transitions in two-dimensional SU(N) Heisenberg models with multispin interactions. *Phys. Rev. B* 80, 180414(R) (2009).
- Sandvik, A. W. Continuous quantum phase transition between an antiferromagnet and a valence-bond solid in two dimensions: evidence for logarithmic corrections to scaling. *Phys. Rev. Lett.* 104, 177201 (2010).
- Chen, K. et al. Deconfined criticality flow in the Heisenberg model with ring-exchange interactions. *Phys. Rev. Lett.* 110, 185701 (2013).
- Harada, K. et al. Possibility of deconfined criticality in SU(N) Heisenberg models at small N. Phys. Rev. B 88, 220408(R) (2013).
- 13. Block, M. S., Melko, R. G. & Kaul, R. K. Fate of  $CP^{N-1}$  fixed points with q monopoles. *Phys. Rev. Lett.* **111**, 137202 (2013).
- Pujari, S., Damle, K. & Alet, F. Néel-state to valence-bond-solid transition on the honeycomb lattice: evidence for deconfined criticality. *Phys. Rev. Lett.* 111, 087203 (2013).
- Nahum, A., Chalker, J. T., Serna, P., Ortuño, M. & Somoza, A. M. Deconfined quantum criticality, scaling violations, and classical loop models. *Phys. Rev. X* 5, 041048 (2015).
- Shao, H., Guo, W. & Sandvik, A. W. Quantum criticality with two length scales. Science 352, 213–216 (2016).
- Zayed, M. et al. 4-Spin plaquette singlet state in the Shastry–Sutherland compound SrCu<sub>2</sub>(BO<sub>3</sub>)<sub>2</sub>. Nat. Phys. 13, 962–966 (2017).
- 18. Shastry, B. S. & Sutherland, B. Exact ground state of a quantum mechanical antiferromagnet. *Physica B+C* **108**, 1069–1070 (1981).
- Corboz, P. & Mila, F. Tensor network study of the Shastry-Sutherland model in zero magnetic field. *Phys. Rev. B* 87, 115144 (2013).
- Nahum, A., Serna, P., Chalker, J. T., Ortuño, M. & Somoza, A. M. Emergent SO(5) symmetry at the Néel to valence-bond-solid transition. *Phys. Rev. Lett.* 115, 267203 (2015).
- 21. Karch, A. & Tong, D. Particle-vortex duality from 3D bosonization. *Phys. Rev. X* **6**, 031043 (2016).
- Metlitski, M. A. & Vishwanath, A. Particle-vortex duality of two-dimensional Dirac fermion from electric-magnetic duality of three-dimensional topological insulators. *Phys. Rev. B* 93, 245151 (2016).
- Mross, D. F., Alicea, J. & Motrunich, O. I. Explicit derivation of duality between a free Dirac cone and quantum electrodynamics in (2+1) dimensions. *Phys. Rev. Lett.* 117, 016802 (2016).
- Kachru, S., Mulligan, M., Torroba, G. & Wang, H. Non-supersymmetric dualities from mirror symmetry. *Phys. Rev. Lett.* 118, 011602 (2017).
- Wang, C., Nahum, A., Metlitski, M. A., Xu, C. & Senthil, T. Deconfined quantum critical points: symmetries and dualities. *Phys. Rev. X* 7, 031051 (2017).
- 26. Qin, Y. Q. et al. Duality between the deconfined quantum-critical point and the bosonic topological transition. *Phys. Rev. X* 7, 031052 (2017).
- Sato, T., Hohenadler, M. & Assaad, F. F. Dirac fermions with competing orders: non-Landau transition with emergent symmetry. *Phys. Rev. Lett.* 119, 197203 (2017).
- Metlitski, M. A. & Thorngren, R. Intrinsic and emergent anomalies at deconfined critical points. *Phys. Rev. B* 98, 085140 (2018).
- Gazit, S., Assaad, F. F., Sachdev, S., Vishwanath, A. & Wang, C. Confinement transition of Z<sub>2</sub> gauge theories coupled to massless fermions: emergent QCD3 and SO(5) symmetry. *Proc. Natl Acad. Sci. USA* 115, E6987 (2018).
- Sreejith, G. J., Powell, S. & Nahum, A. Emergent SO(5) symmetry at the columnar ordering transition in the classical cubic dimer model. *Phys. Rev. Lett.* 122, 080601 (2019).
- Irkhin, V. Yu & Katanin, A. A. Thermodynamics of isotropic and anisotropic layered magnets: renormalization-group approach and 1/N expansion. *Phys. Rev. B* 57, 379–391 (1998).
- 32. Cuccoli, A., Roscilde, T., Tognetti, V., Vaia, R. & Verrucchi, P. Quantum Monte Carlo study of *S*=½ weakly anisotropic antiferromagnets on the square lattice. *Phys. Rev. B* **67**, 104414 (2003).
- Sandvik, A. W. & Evertz, H. G. Loop updates for variational and projector quantum Monte Carlo simulations in the valence-bond basis. *Phys. Rev. B* 82, 024407 (2010).

- Sandvik, A. W. Computational studies of quantum spin systems. AIP Conf. Proc. 1297, 135–338 (2010).
- 35. Sandvik, A. W. Finite-size scaling and boundary effects in two-dimensional valence-bond solids. *Phys. Rev. B* **85**, 134407 (2012).
- Senthil, T. & Fisher, M. P. A. Competing orders, nonlinear sigma models, and topological terms in quantum magnets. *Phys. Rev. B* 74, 064405 (2006).
- Luck, J. M. Corrections to finite-size-scaling laws and convergence of transfer-matrix methods. *Phys. Rev. B* 31, 3069–3083 (1985).
- Vollmayr, K., Reger, J. D., Scheucher, M. & Binder, K. Finite size effects at thermally-driven first order phase transitions: a phenomenological theory of the order parameter distribution. Z. Phys. B 91, 113–125 (1993).
- Iino, S., Morita, S., Sandvik, A. W. & Kawashima, N. Detecting signals of weakly first-order phase transitions in two-dimensional Potts models. *J. Phys. Soc. Jpn* 88, 034006 (2019).
- 40. Sen, A. & Sandvik, A. W. Example of a first-order Néel to valence-bond-solid transition in two dimensions. *Phys. Rev. B* **82**, 174428 (2010).
- Kuklov, A., Prokof'ev, N. & Svistunov, B. Weak first-order superfluid-solid quantum phase transitions. *Phys. Rev. Lett.* 93, 230402 (2004).
- Pelissettp, A. & Vicari, E. Multicritical behavior of two-dimensional anisotropic antiferromagnets in a magnetic field. *Phys. Rev. B* 76, 024436 (2007).
- 43. Hasenbusch, M. & Vicari, E. Anisotropic perturbations in three-dimensional O(*N*)-symmetric vector models. *Phys. Rev. B* **84**, 125136 (2011).
- Eichorn, A., Mesterházy, D. & Scherer, M. M. Multicritical behavior in models with two competing order parameters. *Phys. Rev. E* 88, 042141 (2013).
- Hébert, F. et al. Quantum phase transitions in the two-dimensional hardcore boson model. *Phys. Rev. B* 65, 014513 (2001).
- 46. Demler, E., Hanke, W. & Zhang, S.-C. SO(5) theory of antiferromagnetism and superconductivity. *Rev. Mod. Phys.* **76**, 909–974 (2004).
- 47. Wildeboer, J., D'Emidio, J. & Kaul, R. K. Emergent symmetry at a transition between intertwined orders in a *S*=1 magnet. Preprint at https://arxiv.org/abs/1808.04731 (2018).
- Serna, P. & Nahum, A. Emergence and spontaneous breaking of approximate O(4) symmetry at a weakly first-order deconfined phase transition. Preprint at https://arxiv.org/abs/1805.03759 (2018).
- Muller, M. E. A note on a method for generating points uniformly on n-dimensional spheres. Commun. ACM 2, 19–20 (1959).

#### Acknowledgements

The authors thank F. Assaad, R. Kaul, N. Kawashima, S. Li, Z.Y. Meng, A. Nahum, Y. Ran, S. Sachdev, H. Shao, L. Sun, J. Takahashi and Z.-C. Yang for stimulating discussions. This work was supported by the NSF under grant no. DMR-1710170 and by a Simons Investigator Award. The calculations were carried out on Boston University's Shared Computing Cluster.

#### **Author contributions**

A.W.S. conceived the CBJQ model and planned the study. The numerical simulations of the CBJQ model were implemented and carried out by B.Z. P.W. simulated the classical Heisenberg model. B.Z. analysed all data under the supervision of A.W.S. and with input from P.W. B.Z. wrote the initial draft of the manuscript, which was finalized by A.W.S. with input from B.Z. and P.W.

# Competing interests

The authors declare no competing interests.

## Additional information

**Supplementary information** is available for this paper at https://doi.org/10.1038/s41567-019-0484-x.

Reprints and permissions information is available at www.nature.com/reprints.

Correspondence and requests for materials should be addressed to A.W.S.

**Publisher's note:** Springer Nature remains neutral with regard to jurisdictional claims in published maps and institutional affiliations.

© The Author(s), under exclusive licence to Springer Nature Limited 2019

NATURE PHYSICS ARTICLES

#### Methods

The numerical results for the CBJQ model were obtained by two related QMC methods in which the operator  $e^{-\rho H}$  is Taylor expanded and the resulting powers  $H^n$  are expressed as all possible combinations (propagation paths) of the elementary bond and plaquette operators  $H_i$  of the Hamiltonian. Both methods are well documented in the literature; the SSE method for the standard J–Q model is discussed in detail in ref. <sup>34</sup>, for example, and the projector method is discussed in the context of the S= ½ Heisenberg model in ref. <sup>33</sup> (and useful valence-bond expressions for physical observables of interest are discussed in ref. <sup>30</sup>). Here, we only give very brief overviews and provide specifics related to convergence and the unbiased nature of the simulations.

In the SSE method, which we here run at temperature  $T=\beta^{-1}=1/L$ , paths contributing to the partition function  $Z={\rm Tr}\{e^{-\beta H}\}$  are sampled in the standard basis where the spin components  $S_r^z$  are diagonal. The expansion order (power) n is also sampled as an integral part of this process, and the dominant powers are of order  $\beta N$ . This linear order in N and  $\beta$  also represents the scaling of the computational effort of carrying out one full sweep of Monte Carlo updates. The final results for a given system size are not affected by any approximations beyond statistical errors.

In the valence-bond-based projector method, the ground state is obtained by acting with  $e^{-\beta t l}$ , for  $\beta$  sufficiently large, on a trial state  $|\psi_t\rangle$  expressed in the basis of valence bonds (thus restricting the sampling of paths to the singlet sector). The sampling is carried out in the space of paths contributing to the normalization  $\langle \psi_t|e^{-2\beta t l}|\psi_t\rangle$ , with the spins compatible with the valence bonds in the trial state; that is, the sampling is done with the  $S_t^z$  spins as in SSE, but the operator expectation values are computed purely in the valence bond basis (which corresponds to summing over all possible spin paths contributing to a given sequence of operators). For the trial state, we use an amplitude-product state<sup>51</sup> with bond amplitudes of the form  $h(r) = r^{-3}$ , which produces a good variational state for a 2D system with AFM order. We ensured convergence to the ground state by comparing results for different values of the projection parameter  $\beta$  of the form  $\beta = aL$ . For the largest system sizes around the AFM–PSS transition point (where the convergence is the slowest), we see small differences between results with  $a = \frac{1}{2}$ , 1, 2 and 4, but no statistically discernible differences between results with a = 4 and a = 8 up

to the largest system sizes studied. Once sufficiently converged, the ground-state properties are exact to within statistical errors.

In practice, the technical differences between the SSE and projector methods are rather minor, amounting essentially to different boundary conditions in the time dimension—periodic boundaries for SSE and open boundaries 'capped' by the trial state expressed in the valence bond basis in the projector method. Therefore, the efficient loop updates as described for the J-Q model within the SSE method in ref. <sup>34</sup> can be directly taken over into the projector approach. These loop updates are also very similar to those previously developed for the Heisenberg model<sup>33</sup>. The exclusion of half of the Q terms to go from the standard J-Q model to the CBJQ model is trivial. Both methods were tested against exact diagonalization results for small systems.

We studied the classical 3D Heisenberg model using standard Monte Carlo simulations. To deal with the anisotropy when  $\Delta \neq 1$ , we evolve the spin configurations using hybrid updates. These updates alternate between Metropolis sweeps of  $N=L^3$  single-spin updates and Wolff cluster updates, the latter of which act only on the component of the spins along the z axis $^{52}$ . The cluster updates can also be done on the x-y plane components of the spins; however, we did not see any noticeable difference in performance (and identical results are produced) between the two methods in the neighbourhood of the XY–Ising transition at  $\Delta=1$ . The program was tested against known benchmarks.

## Data availability

The data that support the plots within this paper and other findings of this study are available from the corresponding author upon reasonable request.

## References

- Beach, K. S. D. & Sandvik, A. W. Some formal results for the valence bond basis. Nucl. Phys. B 750, 142–178 (2006).
- Liang, S., Doucot, B. & Anderson, P. W. Some new variational resonatingvalence-bond-type wave functions for the spin-½ antiferromagnetic Heisenberg model on a square lattice. *Phys. Rev. Lett.* 61, 365–368 (1988).
- 52. Wolff, U. Collective Monte Carlo updating for spin systems. *Phys. Rev. Lett.* **62**, 361–364 (1989).